Symmetric Differential Demodulation-Based Heterodyne Laser Interferometry Used for Wide Frequency-Band Vibration Calibration

Ming Yang, *Member, IEEE*, Chenguang Cai, Deguang Wang, Qinmu Wu, Zhihua Liu, and Ying Wang

***Abstract*—The accelerometers are commonly applied to measure the vibrations in the fields of motion control and precision measurement, whose sensitivities are essentially important to their applications. The vibration calibration is utilized to determine their sensitivities before they are used or after a period of time. At present, the Nyquist sampling (NS), bandpass sampling (BPS), and mixer and low-pass filter sampling (MLPFS) based heterodyne laser interferometry are widely utilized to accomplish the vibration calibration. Compared with the NS method, the latter two methods can significantly reduce the sampling rate and extend the calibration frequency range. However, the BPS method has to adopt the complex algorithm and prior information so as to get its sampling rate, and the MLPFS method is inevitably influenced by an extra phase delay. In this article, a novel heterodyne laser interferometry is investigated to simultaneously determine the sensitivity magnitude and phase of the accelerometers with high accuracy in a wide frequency range. This method significantly eliminates the phase delay by introducing an appropriate symmetric differential demodulation strategy, which can improve the sensitivity phase calibration accuracy, especially at higher frequencies. The comparison experiments with the Earth's gravitation and monocular vision methods at low frequencies and the traditional MLPFS and NS methods confirm that the investigated method can calibrate the sensitivity magnitude and phase of accelerometers with the uncertainties of about 0.5% and 0.5° in the range from 0.1 Hz to 20 kHz.**

***Index Terms*—Accelerometers, heterodyne laser interferometry (TLI), sensitivity phase, symmetric differential demodulation (SDD), vibration calibration.**

Manuscript received 15 April 2023; revised 16 June 2023 and 8 July 2023; accepted 16 July 2023. This work was supported in part by the National Natural Science Foundation of China under Grant 52265066, Grant 62203132, Grant 52075512, and Grant 52267003; in part by the National Key R&D Program of China under Grant 2017YFF 0205003 and Grant 2022YFF0609400; in part by the Youth Science and Technology Talents Development Project of Guizhou Education Department under Grant Qianjiaohe KY [2022]138; in part by the Guizhou Provincial Science and Technology Projects under Grant Qiankehejichu [ZK[2022]Yiban103]; in part by the Science and Technology Fund of Guizhou University under Grant Guidateganghezi [2021]04; and in part by the Doctor Foundation Project of Guizhou University under Grant GDRJ [2020]30. *(Corresponding authors: Qinmu Wu; Zhihua Liu.)*

Ming Yang, Deguang Wang, and Qinmu Wu are with the Department of Automation, College of Electrical Engineering, Guizhou University, Guiyang 550025, China (e-mail: myang23@gzu.edu.cn; dgwang@gzu.edu.cn; qmwu@gzu.edu.cn).

Chenguang Cai and Zhihua Liu are with the Institute of Mechanics and Acoustic Metrology, National Institute of Metrology, Beijing 100029, China (e-mail: caichenguang@nim.ac.cn; liuzhihua@nim.ac.cn).

Ying Wang was with the Beijing University of Chemical Technology, Beijing 100029, China. She is now with the Institute of Microelectronics, Chinese Academy of Sciences, Beijing 100029, China, and also with the University of Chinese Academy of Sciences, Beijing 100049, China (e-mail: wangying1@ime.ac.cn).

Color versions of one or more figures in this article are available at https://doi.org/10.1109/TIE.2023.3299015.

Digital Object Identifier 10.1109/TIE.2023.3299015

I. Introduction

THE different types of accelerometers, such as piezoelectric, optomechanical, and micro-electro-mechanical systems (MEMS) have been increasingly used in the applications of seismic warning, civil structural health testing, rail and machine health motioning, medical assistance diagnosing, etc. [1], [2], [3], [4]. The sensitivities of the accelerometers are taken as precision known values in the applications, which directly determines the validity of their measurement data. In order to guarantee the performance of these applications, the accelerometers must be accurately calibrated. Therefore, it is very important to develop an appropriate vibration calibration method for determining the sensitivities of accelerometers in a wide frequency range.

Currently, the laser interferometry (LI) recommended by the International Standard Organization (ISO) [5], [6] is the preferred method to calibrate the accelerometers. The LI can be divided into the two types of homodyne laser interferometry (MLI) and heterodyne laser interferometry (TLI) by the difference of used interferometer. The MLI uses two mutually orthogonal signals that contain the excitation displacement to accomplish the calibration of the accelerometers, which is able to obtain a considerable accuracy in a relatively wide frequency range and its lower frequency can be easily less than 1 Hz [7], [8], such as Veldman [9] presented the MLI based on phase unwrapping method to calibrate the accelerometers, whose uncertainty is less than 1.5% in the range of 10 Hz–10 kHz. Lee et al. [10] used the harmonic components of a homodyne interference signal to achieve the sensitivity phase calibration, which can get the uncertainty of 0.25° in the range of 40 Hz–10 kHz. Garg et al. [11] utilized the discrete Fourier transform-based MLI to calibrate the accelerometers, and its accuracy can reach 1.4% at frequencies between 0.1 Hz and 20 kHz. Scott and Dickinson [12] investigated an MLI that considers the distortion effects in the low-frequency calibration, whose uncertainty is

limited to 0.2% in the 0.5–20 Hz. D'Emilia et al. [13] provided a flexible MLI to calibrate the triaxial accelerometer, whose accuracy is about 2%. However, affected by the signal fading and nonlinearity, the MLI failed to determine the sensitivities at the cutoff frequencies of its wide frequency range accurately.

Compared with the MLI, the TLI is increasingly applied to the wide frequency-band vibration calibration because of its advantages in high displacement measurement accuracy, wide dynamic range, low nonlinearity, etc. [14], [15]. The TLI uses a laser interference signal with high carrier frequency to measure the excitation displacement, which has gradually become the hotspot in the vibration calibration [16], [17]. Sun et al. [18] proposed a TLI with the modified sine approximation method (SAM) to calibrate the sensitivity magnitude and phase, which is able to get the accuracy of 1% and 1° in the range of 10 Hz–10 kHz, respectively. Yang et al. [19] investigated a TLI that is based on the bandpass sampling (BPS) theorem to efficiently measure the excitation displacement in the range from 5 Hz to 20 kHz, whose amplitude and phase standard deviations are superior to 0.1% and 0.1°. Wang et al. [20] improved the performance of the TLI by considering the influences of periodic nonlinear errors, whose displacement measurement accuracy can highly reach 0.1 nm. Zhai et al. [21] utilized the TLI to calibrate the accelerometers at medium frequencies with especially high acceleration, and its accuracy is approximately 0.3%. Yang et al. [22] used the TLI to accomplish the vibration calibration at ultrahigh frequencies, which can get a similar accuracy compared with most of the National Physical Laboratories. Additionally, Yang et al. [14] applied the TLI with three interferometers to calibrate the triaxial accelerometer, whose accuracies both for the axial and transverse sensitivities are considerable in the range from 5 Hz to 1.6 kHz. In recent two years, the TLI was gradually applied to calibrate the digital accelerometers, whose scale factor and phase-shift calibration accuracies can highly reach 0.2% and 0.1°, respectively [23], [24]. Although the TLI can accomplish the vibration calibration in a relatively wide frequency range, its calibration accuracy and frequency range are usually contradictory.

The calibration performance of TLI depends on its excitation measurement accuracy, which is related to the acquisition and demodulation of the heterodyne laser interference signal [14]. Currently, the commonly used acquisition methods include the Nyquist sampling (NS) method, the BPS method, and the mixer and low-pass filter sampling (MLPFS) method [14], [18], [19]. The NS method is easy to accomplish the high-frequency vibration calibration with high accuracy, while its frequency is limited. Although the BPS method can achieve the calibration in the wide frequency band without any extra analog devices, it requires a complex sampling rate calculation method and a special acquisition card [25]. The MLPFS method utilizes the analog devices to accomplish the wide frequency-band vibration calibration; whose accuracy and efficiency are appropriate [18]. This method is the most widely used and recommended by the different National Institutes of Metrology because of its simplifying nature and flexibility; however, its sensitivity phase is significantly affected by the analog low-pass filter when the frequency is higher than 5 kHz [19]. Additionally, the phase unwrapping and SAMs that are used for the demodulation are optimal, which have been proven by several relevant pieces of literature [26], [27].

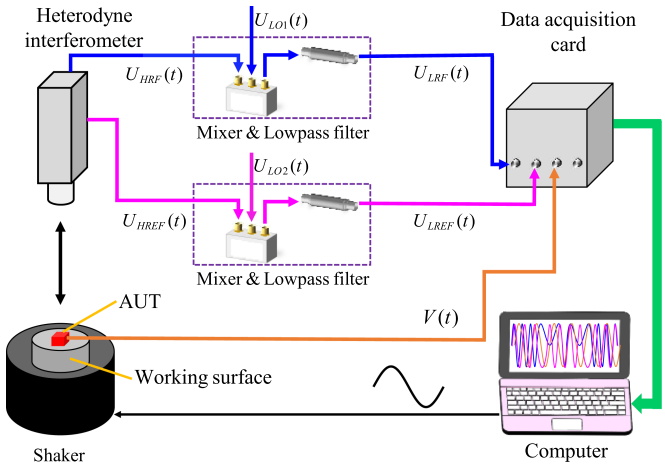

Fig. 1. Schematic drawing of SDD-based heterodyne interferometry calibration system for the accelerometers in the wide frequency range.

To improve the calibration accuracy of the TLI, especially for the sensitivity phase at higher frequencies, a new TLI that is based on symmetric differential demodulation (SDD) is investigated. This method is easily able to eliminate the influence of used analog devices on the sensitivity phase calibration via adopting the SDD strategy, whose calibration frequency can be lower than 1 Hz and up to tens of kHz. Compared with the TLI with the BPS method in our previous articles [14], [19] and the TLI with the NS and MLPFS methods reported by many pieces of literature and recommended by ISOs, the investigated method presents better comprehensive performances in calibration accuracy and efficiency as well as the frequency range. Additionally, the calibration uncertainties of the investigated method for the sensitivity magnitude and phase in the wide frequency range are also evaluated [28], [29], [30], [31].

The rest of this article is organized as follows. Section II depicts the calibration system of the SDD-based heterodyne interferometry. In Section III, the principle of the SDD-based heterodyne interferometry used for calibrating the sensitivity magnitude and phase of the accelerometers is described in detail. Several experimental verifications and results analysis are provided in Section IV. Section V gives the corresponding error sources and calibration uncertainty. Finally, Section VI concludes this article.

II. SDD-Based Heterodyne Interferometry Calibration System for the Accelerometers

Fig. 1 describes a schematic diagram of an SDD-based TLI calibration system for determining the sensitivity magnitude and phase of the accelerometers in the wide frequency range. A shaker provides the vibration excitation in the wide frequency range with specific amplitudes for the accelerometer under test

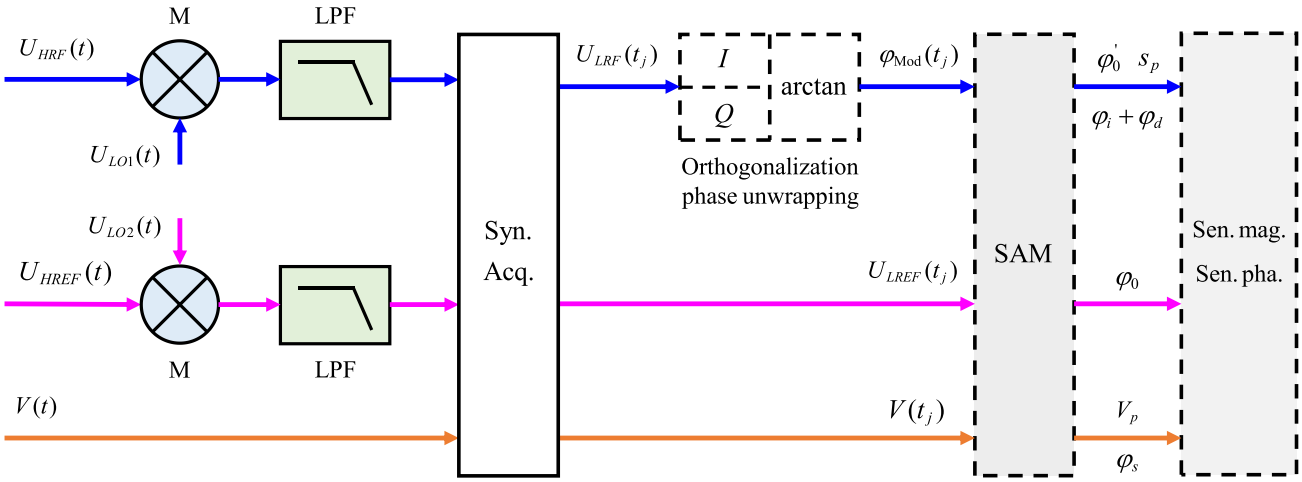

Fig. 2. Flowchart of SDD-based TLI used for the sensitivity magnitude and phase calibration of accelerometers in the wide frequency range.

(AUT). The AUT is firmly mounted on the center of the shaker's working surface, which has consistent excitation with this working surface. A heterodyne interferometer that can directly output the original laser interference signal and reference signal simultaneously is used to measure the excitation acceleration of the AUT, whose laser beam is focused vertically onto the center of the AUTs surface.

Two same types of analog mixer and low-pass filter (MLPF) transform the original laser interference signal and reference signal into the low carrier frequency interference signal and low-frequency reference signal, respectively. The data acquisition (DAQ) card is applied to collect the transformed interference and reference signals as well as the output signal of the AUT simultaneously. The excitation acceleration of the AUT is got by processing the collected interference and reference signals. Ultimately, the sensitivity magnitude and phase of the AUT are determined by calculating the amplitudes and initial phases of the excitation acceleration and the output signal.

Because the shaker is excited by the sinusoidal signal, the original laser interference signal $U_{\mathrm{HRF}}(t)$ and reference signal $U_{\mathrm{HREF}}(t)$ of the heterodyne interferometer can be given by

$$\begin{cases} U_{\mathrm{HRF}}(t) = U_{\mathrm{HRF}} \cos\left[\varphi_{\mathrm{Mod}}(t)\right] \\ U_{\mathrm{HREF}}(t) = U_{\mathrm{HREF}} \cos\left(2\pi f_c t + \varphi_0\right) \end{cases} \tag{1}$$

of which the modulated phase $\varphi_{\mathrm{Mod}}(t)$ and excitation displacement $s(t)$ have the forms

$$\begin{cases} \varphi_{\mathrm{Mod}}(t) = 2\pi f_c t + s(t) \cdot 4\pi/\lambda + \varphi_0 \\ s(t) = s_p \cos\left(2\pi f_v t + \varphi_i\right) \end{cases} \tag{2}$$

where U_{HRF}, f_c, and φ_0 are the amplitude, carrier frequency, and initial phase of $U_{\mathrm{HRF}}(t)$, respectively; U_{HREF} is the amplitude of $U_{\mathrm{HREF}}(t)$. s_p, f_v, and φ_i are the amplitude, frequency, and initial phase of $s(t)$; and λ is the laser wavelength (632.8 nm). The bandwidth B of the $U_{\mathrm{HRF}}(t)$ depends on the corresponding excitation velocity, which is usually much lower than f_c. Therefore, the analog MLPF is applied to achieve the downconversion of $U_{\mathrm{HRF}}(t)$ and $U_{\mathrm{HREF}}(t)$ in order to significantly decrease their required sampling rate.

III. Calibration Principle of the Accelerometers by the SDD-Based Heterodyne Interferometry

A flowchart of SDD-based TLI calibration principle for the sensitivity magnitude and phase of accelerometers is illustrated in Fig. 2. The $U_{\mathrm{HRF}}(t)$ and $U_{\mathrm{HREF}}(t)$ with the frequency f_c are transformed to the $U_{\mathrm{LRF}}(t)$ and $U_{\mathrm{LREF}}(t)$ by the analog MLPFs, whereafter the $U_{\mathrm{LRF}}(t)$ and $U_{\mathrm{LREF}}(t)$ as well as the output signal $V(t)$ of AUT are collected by the DAQ synchronously, which can be expressed as follows:

$$\begin{cases} U_{\mathrm{LRF}}(t_j) = U_{\mathrm{LRF}} \cos \\ \qquad \left[2\pi\left(f_c - f_{\mathrm{LO1}}\right) t_j + s(t_j) \cdot 4\pi/\lambda + \varphi'_0\right] \\ V(t_j) = V_p \cos\left(2\pi f_v t_j + \varphi_s\right) \\ U_{\mathrm{LREF}}(t_j) = U_{\mathrm{LREF}} \cos\left[2\pi\left(f_c - f_{\mathrm{LO2}}\right) t_j + \varphi_0\right] \end{cases} \tag{3}$$

where U_{LRF} and U_{LREF} are the amplitudes of $U_{\mathrm{LRF}}(t)$ and $U_{\mathrm{LREF}}(t)$, f_{LO1} and f_{LO2} are the local frequencies of mixers, φ'_0 is the initial phase affected by the time delay of the low-pass filter, and V_p and φ_s are the amplitude and initial phase of $V(t)$. t_j is the sampling time, $j = 1, 2, \ldots, N$, and N is the sampling number. f_{LO2} can approach f_c infinitely, which makes the frequency of $U_{\mathrm{LREF}}(t)$ much lower than the cutoff frequency of the low-pass filter; thus, the time delay of the low-pass filter on $U_{\mathrm{LREF}}(t)$ can be ignored.

A. Amplitude and Initial Phase Measurement of Excitation Acceleration With High Accuracy

The sensitivity calibration accuracy of AUT depends on the measurement accuracy of the vibration excitation demodulated from the interference signal. In order to obtain the phase $\varphi_{\mathrm{Mod}}(t)$ that is modulated by the sinusoidal excitation displacement from the collected interference signal, the $U_{\mathrm{LRF}}(t_j)$ is first divided into two quadrature signals with an orthogonal basis $< I, Q >$ in the algorithm, which can be calculated by

$$\begin{cases} U_{L1}(t_j) = U_{\mathrm{LRF}}(t_j) \cdot I \\ U_{L2}(t_j) = U_{\mathrm{LRF}}(t_j) \cdot Q \end{cases} \tag{4}$$

of which

$$\begin{cases} I = \sin\left(2\pi f_{or} t_j\right) \\ Q = \cos\left(2\pi f_{or} t_j\right) \end{cases} \tag{5}$$

where f_{or} is the frequency of I and Q. After eliminating the high-frequency components of $U_{L1}(t_j)$ and $U_{L2}(t_j)$ by the digital low-pass filter, they can be simplified to

$$\begin{cases} U_{L1}(t_j) = U_{L1}\cos\left[2\pi f'_{c1} t_j + s\left(t_j\right)\cdot 4\pi/\lambda + \varphi'_0\right] \\ U_{L2}(t_j) = U_{L2}\sin\left[2\pi f'_{c2} t_j + s\left(t_j\right)\cdot 4\pi/\lambda + \varphi'_0\right] \end{cases} \tag{6}$$

where f'_{c1} and f'_{c2} are the carrier frequency of $U_{L1}(t)$ and $U_{L2}(t)$, respectively, which is equal to $f_c - f_{\mathrm{LO1}} - f_{or}$ and $f_c - f_{\mathrm{LO2}} - f_{or}$.

For the two quadrature signals $U_{L1}(t_j)$ and $U_{L2}(t_j)$, the phase unwrapping method is adopted to obtain their modulated phase, which is calculated by the following formula:

$$\varphi'_{\mathrm{Mod}}\left(t_j\right) = \arctan\left[\frac{U_{L2}\left(t_j\right)}{U_{L1}\left(t_j\right)}\right] + k\pi \tag{7}$$

where $k\pi$ is an additional phase that is used to avoid the discontinuities in the $\varphi'_{\mathrm{Mod}}(t)$ caused by the arctan calculation at the zero crossings of $U_{L1}(t_j)$, and the value of k is an integer that belongs to the set $\{0, 1, 2, \ldots\}$.

In order to acquire the amplitude and initial phase of $s(t)$, the SAM with four parameters in [32] and [33] is applied to fit the calculated phases $\{\varphi'_{\mathrm{Mod}}(t_j)\}$ and corresponding sampling time sequences $\{t_j\}$. The solution process is given as follows:

$$\varphi'_{\mathrm{Mod}}\left(t_j\right) = A_s\cos\left(\omega_v t_j\right) - B_s\sin\left(\omega_v t_j\right) + C_s t_j + D_s \tag{8}$$

where ω_v is the angular frequency. A_s and B_s are the sinusoidal components, C_s is the linear component caused by the carrier frequency, and D_s is the offset component. The C_s is utilized to eliminate the influences of clock jitter and carrier frequency instability that leads to the variation of f_c, and the D_s is used to remove offset components at different sampling times. The N phases $\{\varphi'_{\mathrm{Mod}}(t_j)\}$ and their corresponding time $\{t_j\}$ constitute the overdetermined equations, where N is much greater than 4. These equations can be converted into the matrix form

$$\begin{bmatrix} \varphi'_{\mathrm{Mod}}\left(t_1\right) \\ \varphi'_{\mathrm{Mod}}\left(t_2\right) \\ \vdots \\ \varphi'_{\mathrm{Mod}}\left(t_N\right) \end{bmatrix} = \begin{bmatrix} \cos\left(\omega_v t_1\right) & -\sin\left(\omega_v t_1\right) & t_1 & 1 \\ \cos\left(\omega_v t_2\right) & -\sin\left(\omega_v t_2\right) & t_2 & 1 \\ \vdots & \vdots & \vdots & \vdots \\ \cos\left(\omega_v t_N\right) & -\sin\left(\omega_v t_N\right) & t_N & 1 \end{bmatrix} \times \begin{bmatrix} A_s \\ B_s \\ C_s \\ D_s \end{bmatrix} \tag{9}$$

the parameters A_s, B_s, C_s, and D_s can be solved by using the least square method. The fitted amplitude and initial phase of $s(t)$ can be calculated by the solved A_s and B_s with the following formula:

$$\begin{cases} s_p = \frac{\lambda}{4\pi}\sqrt{A_s^2 + B_s^2} \\ \varphi_i = \arctan\left(\frac{B_s}{A_s}\right) + \varphi_d \end{cases} \tag{10}$$

where φ_d is the phase delay caused by the time delay of a low-pass filter.

Furthermore, the corresponding excitation acceleration amplitude a_p and initial phase φ_a can be obtained by the following second derivative equation:

$$\begin{cases} a_p = \omega_v^2 s_p \\ \varphi_a = \varphi_i + \pi \end{cases} \tag{11}$$

similarly, the collected reference signal $U_{\mathrm{LREF}}(t_j)$ and $V(t_j)$ are also fitted by the SAM, as shown in (8), respectively. The corresponding parameters A_R and B_R, and A_V and B_V can be obtained by using (9), whereafter the initial phase φ_0 of $U_{\mathrm{LREF}}(t)$ as well as the fitted amplitude V_p and initial phase φ_s of $V(t)$ can be calculated by

$$\begin{cases} \varphi_0 = \arctan\left(B_R/A_R\right) \\ V_p = \sqrt{A_V^2 + B_V^2} \\ \varphi_s = \arctan\left(B_V/A_V\right). \end{cases} \tag{12}$$

B. Sensitivity Magnitude and Phase Calibration of the Accelerometer

The time delay caused by the low-pass filter inevitably affects the initial phase of the excitation acceleration, which leads to the φ_d, as shown in (10). This delay reduces the sensitivity phase calibration accuracy, especially at high frequencies. Combining (3), (7), and (8), φ_d can be determined by the proposed symmetric differential way with the formula

$$\varphi_d = \varphi'_0 - \varphi_0 \tag{13}$$

where φ'_0 is the solved parameter D_s in (8).

According to the sensitivity definition in ISO, the sensitivity magnitude S_{mag} is the ratio of the fitted amplitude of $V(t)$ to that of the excitation acceleration, and the sensitivity phase S_{pha} is the difference of the initial phases between the output signal and excitation acceleration. Therefore, the S_{mag} and S_{pha} can be calculated by

$$\begin{cases} S_{\mathrm{mag}} = V_p/a_p \\ S_{\mathrm{pha}} = \varphi_s - \varphi_a + \varphi_d. \end{cases} \tag{14}$$

Additionally, the relative standard deviation ($S_{m,\,\mathrm{RStd}}$) of S_{mag} and the standard deviation ($S_{p,\,\mathrm{Std}}$) of S_{pha}, as shown in (15), are introduced to describe the calibration repeatability of the investigated method

$$\begin{cases} S_{m,\mathrm{RStd}} = \mathrm{Std.}\left(S_{\mathrm{mag}}\right)/\mathrm{Ave.}\left(S_{\mathrm{mag}}\right)\cdot 100\% \\ S_{p,\mathrm{Std}} = \mathrm{Std.}\left(S_{\mathrm{pha}}\right). \end{cases} \tag{15}$$

IV. Experimental Verifications and Results Analysis

The SDD-based TLI calibration system used for determining the sensitivity magnitude and phase of accelerometers in the wide frequency range was set up according to the schematic drawing in Fig. 1, as displayed in Fig. 3.

The two shakers (ESZ185-400 with the range 0.01–100 Hz and PCB 396C11 with the range 5 Hz–20 kHz) were applied to provide the sinusoidal excitation in the range 0.1 Hz–20 kHz, and their provided maximum accelerations were 10 m/s^2 and 100 m/s^2, respectively. The low-frequency AUT (MSV 3000)

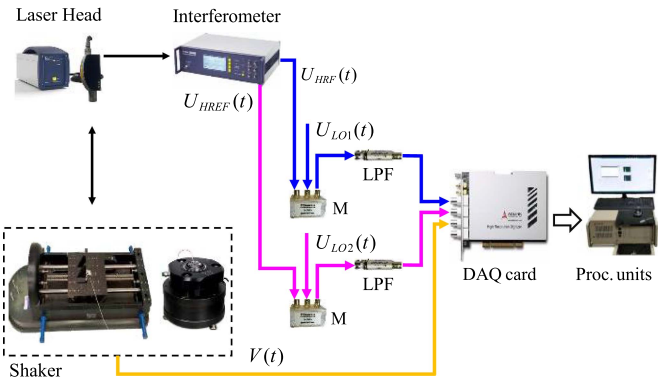

Fig. 3. SDD-based TLI experimental setup for the sensitivity magnitude and phase calibration of accelerometers.

and the embedded AUT in the PCB 396C11 were firmly mounted on the center of the shakers' working surface. The Polytec heterodyne laser interferometer (OFV-5000) with the measurement accuracy of the sub-nanometer was utilized to measure the excitation acceleration. The mixer (MC ZAD-1-1+) with the frequency 0.5–500 MHz and low-pass filter (MC BLP-2.5+) with the cutoff frequency of 2.5 MHz was applied to convert the original laser interference and reference signals. The DAQ card (ADLINK 9846) with the maximum sampling rate of 40 MHz is used to collect the two transformed signals and the output signal of AUT simultaneously.

A. Calibrated Sensitivity Magnitude and Phase Results of Low-Frequency Accelerometer

In order to validate the performance of the investigated SDD-TLI for calibrating the accelerometer at low frequencies, the AUT was calibrated in the range from 0.1 to 10 Hz, and the tested frequency was selected according to the one-third octave regulation. The sensitivity magnitude and phase were calibrated by the SDD-TLI, Earth's gravitation (EG) [32], and monocular vision (MV) methods [33], [34], [35], [36], and they were calibrated ten times at each tested frequency, respectively.

Fig. 4(a) and (d) shows the calibrated sensitivity magnitudes and phases by the EG and MV methods, and the investigated SDD-TLI. In the whole range, the $S_{m,\,\mathrm{Ave}}$ of the SDD-TLI was similar to those of the EG and MV methods, and their corresponding maximum relative deviations were about 0.3% and 0.4%, respectively. The $S_{m,\,\mathrm{RStd}}$ of the SDD-TLI also resembled those of the EG and MV methods in the 0.1–10 Hz, which is less than 0.216%. Although it slightly increased with the decreasing of the frequency in the range of 0.1–0.5 Hz, it is also acceptable compared with the MV method. The calibrated sensitivity phase curve of the SDD-TLI was highly consistent with those of the other two methods. In the range of 0.1–10 Hz, the maximum differences between the SDD-TLI and EG as well as MV methods were 0.067° and 0.183°, respectively. Although the $S_{p,\,\mathrm{Std}}$ of the SDD-TLI was slightly greater than those of the EG and MV methods when the frequency is less than 0.4 Hz, it was similar to those of the EG and MV methods at other higher frequencies.

B. Calibrated Sensitivity Magnitude and Phase Results of Medium- and High-Frequency Accelerometer

To fully verify the calibration accuracy of the investigated SDD-TLI, the sensitivity magnitude and phase of the embedded AUT at frequencies between 10 Hz and 20 kHz were calibrated by the SDD-TLI, NS-TLI, and traditional MLPFS-TLI simultaneously. The sensitivity magnitude and phase were calibrated ten times at each tested frequency in this range. Fig. 5 shows the sensitivity magnitude and phase calibrated by the MLPFS- TLI, SDD-TLI, and NS-TLI. The calibrated $S_{m,\,\mathrm{Ave}}$ of the SDD-TLI kept a highly similar trend with those of the NS-TLI and MLPFS-TLI, and their corresponding relative deviations were less than 0.866% and 0.375%, respectively. The maximum $S_{m,\,\mathrm{RStd}}$ of the SDD-TLI was 0.086% in the 10 Hz–20 kHz, which is slightly less than the corresponding 0.112% of the MLPFS-TLI and 0.101% of the NS-TLI, respectively. The maximum difference of the $S_{p,\,\mathrm{Ave}}$ between the SDD-TLI and NS-TLI was about 0.1°, which is less than the corresponding 0.811° between the MLPFS-TLI and NS-TLI. The $S_{p,\,\mathrm{Std}}$ of the SDD-TLI was highly similar to those of the SDD-TLI and MLPFS-TLI, and it was less than 0.1° except at a few higher frequencies.

C. Discussion

In order to further illustrate the calibration performance of the investigated SDD-TLI, the range of 0.1 Hz–20 kHz was split to four ranges, as listed in Table I. As shown in Fig. 4(a), the sensitivity magnitude of the SDD-TLI was greater than that of the EG method because the latter is inevitably affected by the centrifugal acceleration in the range from 2 to 10 Hz. The MV method appeared larger sensitivity magnitude than that of the SDD-TLI because it requires more time to calibrate the AUT, and such will increase the temperature drift. There were maximum differences of 0.3% and 0.4% existed among the SDD-TLI and the EG method as well as the MV method, which can be acceptable compared with the current calibration accuracy for the low-frequency accelerometers. As displayed in Fig. 4(b) and (d), the standard deviations of these three methods were increased as the decreasing of the frequency in the very low frequency range because the SNR of the AUTs output signal is gradually insufficient. In the 0.1–0.3 Hz, the SDD-TLI has obvious standard deviations both for the sensitivity magnitude and phase than those of the EG and MV methods. The reason for this trend is due to the SDD-TLI inevitably influenced by the weak collimation, slight excitation velocity, and speckle noise when it is applied to measure the vibration in this range. As the frequency increases in the range from 0.3 to 10 Hz, the standard deviations of the SDD-TLI decrease since these influences can be dramatically reduced in this range.

As shown in Fig. 5(a), the SDD-TLI and the MLPFS-TLI as well as the NS-TLI presented the highly consistent trends. The maximum relative standard deviation of the SDD-TLI was 0.086% because it has enough resolution and stability in the whole range. As displayed in Fig. 5(c), the difference of the SDD-TLI and NS-TLI is negligible, while its difference with the MLPFS-TLI gradually increased as the increasing of the

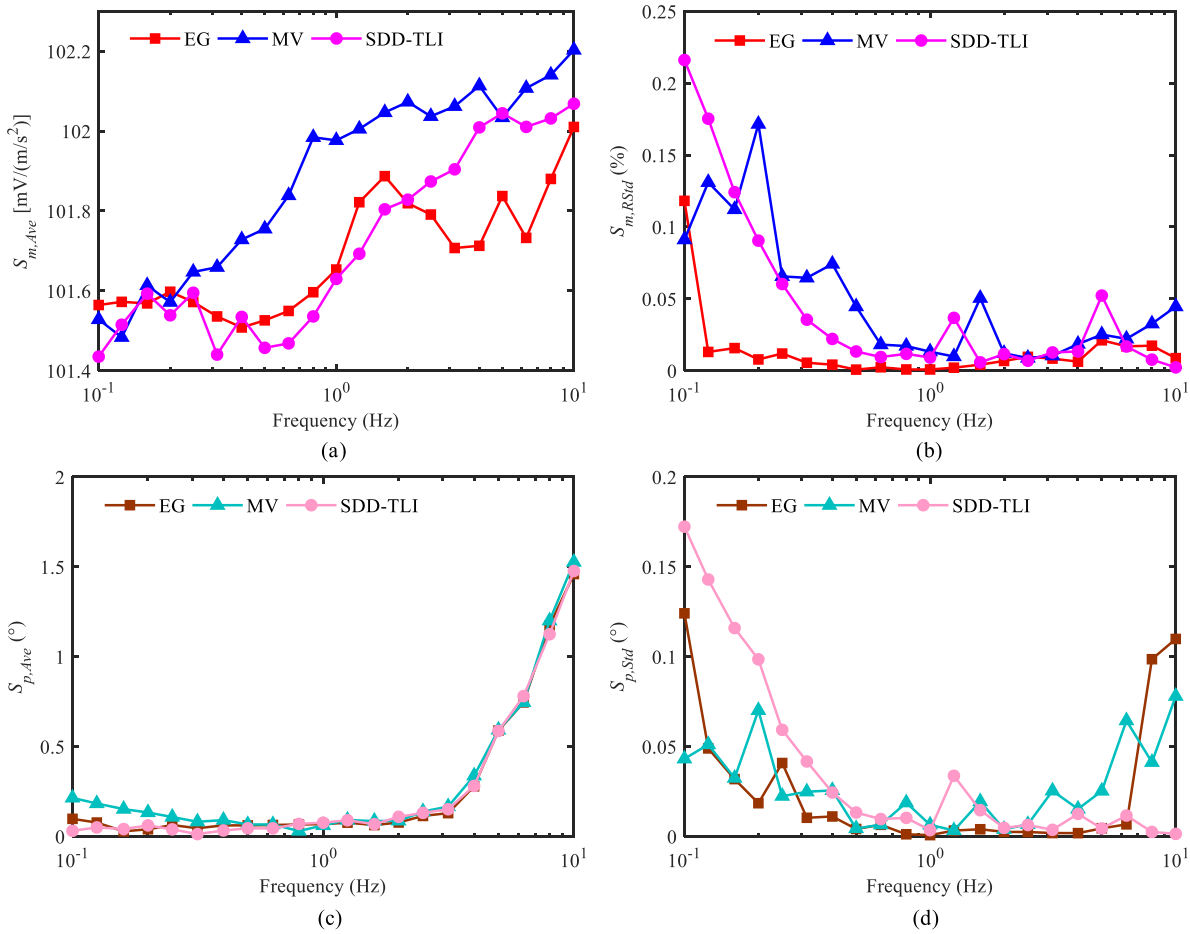

Fig. 4. Calibrated sensitivity magnitude and phase of the low-frequency AUT by the investigated SDD-TLI, MV, and EG methods in the range of 0.1–10 Hz. (a) Average value ($S_{m,\ \mathrm{Ave}}$) of sensitivity magnitude. (b) $S_{m,\ \mathrm{RStd}}$ of sensitivity magnitude. (c) $S_{p,\ \mathrm{Ave}}$ of sensitivity phase. (d) $S_{p,\ \mathrm{Std}}$ of sensitivity phase.

TABLE I
REPEATABILITY OF CALIBRATED SENSITIVITY MAGNITUDE AND PHASE OF ACCELEROMETER BY THE INVESTIGATED SDD-TLI, MLPFS-TLI, EG METHOD, AND MV METHOD IN THE RANGE FROM 0.1 HZ TO 20 KHZ

Frequency range	SDD-TLI		MLPFS-TLI		EG method		MV method	
	$S_{m,Rstd}$ (%)	$S_{p,Std}$ (°)	$S_{m,Rstd}$ (%)	$S_{p,Std}$ (°)	$S_{m,Rstd}$ (%)	$S_{p,Std}$ (°)	$S_{m,Rstd}$ (%)	$S_{p,Std}$ (°)
0.1 Hz ≤ f_v < 0.3 Hz	0.216	0.172	—	—	0.118	0.124	0.172	0.070
0.3 Hz ≤ f_v < 10 Hz	0.052	0.042	—	—	0.021	0.110	0.074	0.078
10 Hz ≤ f_v ≤ 10 kHz	0.086	0.173	0.112	0.222	—	—	—	—
10 kHz < f_v ≤ 20 kHz	0.078	0.535	0.063	0.587	—	—	—	—

frequency when it is greater than 5 kHz. The reason for this phenomenon is that the phase delay caused by the low-pass filter can be ignored at low frequencies, while it is significant at high frequencies. The relatively large standard deviation appeared at a few high frequencies because the AUT at these frequencies cannot guarantee the high-SNR output signal.

The low cutoff frequency of the investigated SDD-TLI was limited to 0.1 Hz in this experiment since the used DAQ card cannot collect the signal for enough long time influenced by its memory. The frequency of this method even can be lower than 0.1 Hz if an appropriate DAQ card with large memory is used. Correspondingly, the upper frequency of the SDD-TLI can also be easily higher than 20 kHz if the tested accelerometer is able to output the signal with high SNR.

V. MEASUREMENT UNCERTAINTY

In order to further illustrate the accuracy of the investigated method, its measurement uncertainty for the sensitivity calibration of the accelerometer was accomplished. The generation and measurement of excitation acceleration, the measurement of AUTs output signal, the external vibration and noises, and the sensitivity repeatability in the whole calibration procedure were considered as the main error sources, as provided in Table II. The corresponding uncertainty components $\{u_{\ \mathrm{rel},\ i}\}$ of these sources can be evaluated by the recommended methods in guide to the expression of uncertainty in measurement (GUM) [37] according to their probability density distributions. Then, the relative contribution (Rel. contr.) of each error source is the

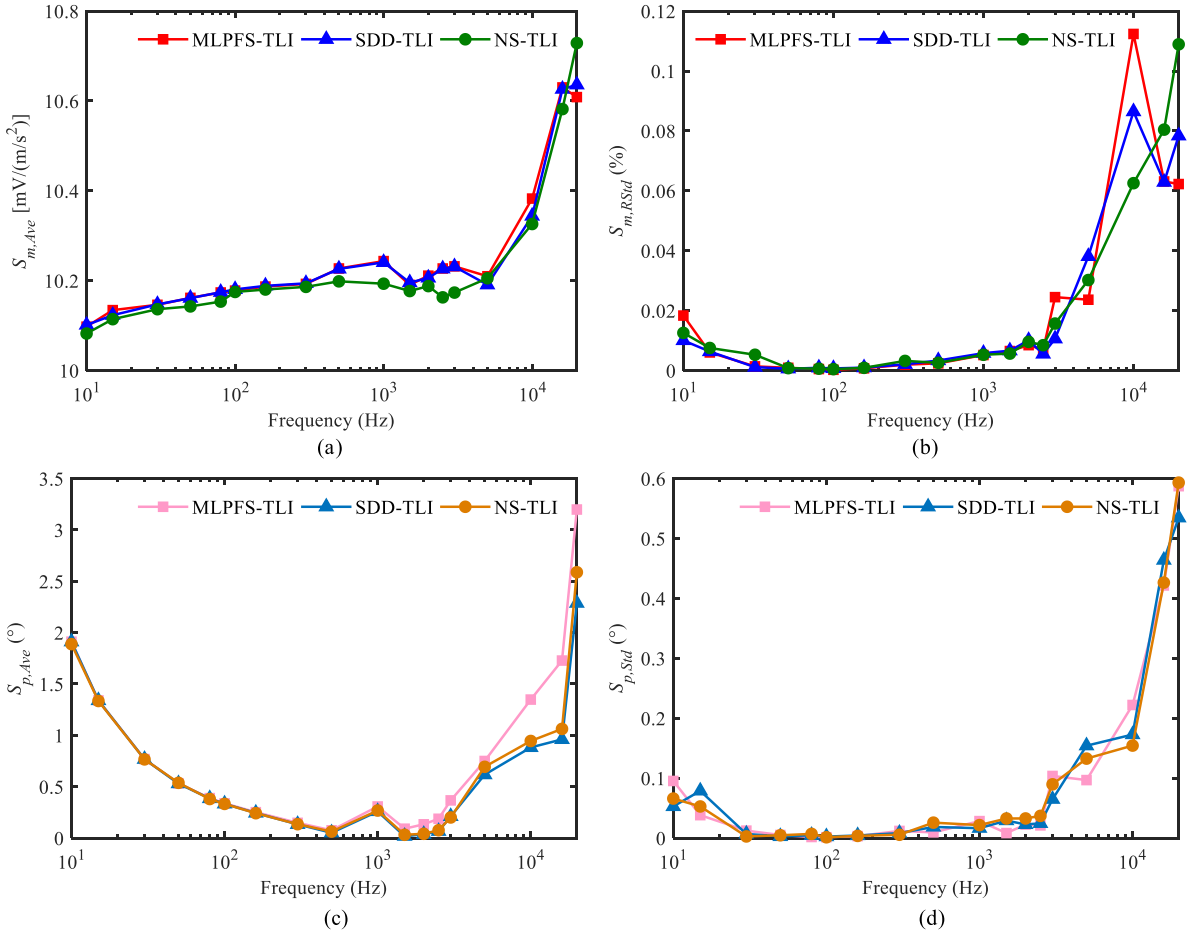

Fig. 5. Sensitivity magnitude and phase of the medium- and high-frequency AUT calibrated by the investigated method, MLPFS-TLI, and NS-TLI in the range from 10 Hz to 20 kHz. (a) $S_{m,\,\mathrm{Ave}}$ of sensitivity magnitude. (b) $S_{m,\,\mathrm{RStd}}$ of sensitivity magnitude. (c) $S_{p,\,\mathrm{Ave}}$ of sensitivity phase. (d) $S_{p,\,\mathrm{Std}}$ of sensitivity phase.

TABLE II
UNCERTAINTY SOURCES AND THEIR CORRESPONDING UNCERTAINTIES OF THE INVESTIGATED SDD-TLI FOR THE ACCELEROMETERS CALIBRATION IN THE WIDE FREQUENCY RANGE

No.	Symbol	Error sources	Component	Distribution	d_i	c_i	Rel. contr.
		Uncertainty caused by the generation and measurement of excitation acceleration					
1	u (no)	Effect of the noises on the interference signal measurement	0.05%	Rectangle	1.73	1	0.0289%
2	u (fi)	Effect of the filters on the interference signal measurement	0.01%	Rectangle	1.73	1	0.0058%
3	u (vo)	Effect of the voltage on the interference signal measurement	0.05%	Rectangle	1.73	0.01	0.0003%
4	u (vb)	Effect of the vibration on the interference signal measurement	0.10%	Rectangle	1.73	1	0.0578%
5	u (pn)	Effect of the phase noise on the interference signal measurement	0.01%	Rectangle	1.73	1	0.0058%
6	u (of)	Other effects of on the interference signal measurement	0.03%	Rectangle	1.73	1	0.0173%
7	u (fg)	Measurement uncertainty of the vibration frequency	0.05%	Rectangle	1.73	1	0.0289%
8	u (es)	Measurement uncertainty of the laser wavelength	2.5E-11 nm	Normal	2	100	0.0001%
9	u (st)	Effect of the transverse motion on the interference signal measurement	0.04%	Rectangle	1.73	1	0.0231%
10	u (en)	Effect of the external noises on the interference signal measurement	0.05	Rectangle	1.73	1	0.0289%
11	u (fp)	Effect of the laser focus position on the interference signal measurement	0.02%	Rectangle	1.73	1	0.0116%
		Uncertainty caused by the calibration of accelerometer					
12	u (ea)	Effect of the non-alignments between the geometrical axes	0.03%	Rectangle	1.73	1	0.0173%
13	u (us)	Measurement uncertainty of the output signal of AUT	0.05%	Rectangle	1.73	1	0.0289%
14	u (rm)	Effect of the rigid modal on the output signal measurement	0.04%	Rectangle	1.73	1	0.0231%
15	u (et)	Effect of the temperature on the output signal measurement	0.05%	Rectangle	1.73	1	0.0289%
16	u (rs)	Repeatability of the output signal measurement	0.10%	Normal	2	1	0.0500%
17	u (eo)	Other effects on the output signal measurement	0.10%	Rectangle	1.73	1	0.0578%
18	u (rp)	Repeatability of the calibrated sensitivity magnitude	0.216%	Normal	1	1	0.2160%
	u (s_m)	Combined calibration uncertainty		$k=1$			0.2479%
	U (s_m)	Expanded calibration uncertainty ($k=2$)		$k=2$			0.4962%

ratio of its $u_{\text{rel},\,i}$ to the corresponding probability distribution divisor d_i. The combined calibration uncertainty $U_{\text{rel}}(S)$ that consider the Rel. contr. of the whole error sources according to the propagation criterion can be given by

$$U_{\text{rel}}(S) = \sum_{i=1}^{M} \frac{c_i \cdot u_{\text{rel},i}}{d_i} \tag{16}$$

where c_i is the corresponding sensitive coefficient. Therefore, the expanded calibration uncertainty of sensitivity magnitude is $U_{\text{rel}}(S)$ multiplies the coverage factor k that means a confidence interval, which was 0.496%. Similarly, the expanded calibration uncertainty of the sensitivity phase was 0.422° in the range from 0.1 Hz to 10 kHz. Compared with the reported uncertainty of HLI and TLI in the pieces of literature [11], [18], [30], the investigated SDD-TLI can meet the high-accuracy calibration demand of the accelerometers in the wide frequency range.

VI. Conclusion

In this article, we investigated a novel SDD-based TLI for determining the sensitivity magnitude and phase of accelerometers in the wide frequency range, which can improve the accuracy, especially for the sensitivity phase at high frequencies. The investigated method determined the sensitivity magnitude and phase by applying the symmetric MLPFS that is composed of the analog mixer and the analog low-pass filter, which can significantly eliminate the extra phase delay by using their differential way. The comparison experiments with the commonly used MV and EG methods in the range of 0.1–10 Hz, and the traditional MLPFS-TLI and NS-TLI in the range of 10 Hz–20 kHz confirm that the investigated SDD-TLI can obtain satisfactory calibration accuracies both for the sensitivity magnitude and phase of accelerometers. Ultimately, the main error sources in the calibration procedure were considered to evaluate the uncertainties, which also demonstrated that the SDD-TLI method has good calibration performance.

References

[1] M. Yang, Z. Liu, C. Cai, Y. Wang, Jing Yang, and J. Yang, "Monocular vision-based calibration method for the axial and transverse sensitivities of low-frequency triaxial vibration sensors with the elliptical orbit excitation," *IEEE Trans. Ind. Electron.*, vol. 69, no. 12, pp. 13763–13772, Dec. 2022, doi: 10.1109/TIE.2021.3130325.

[2] T. Deng, D. Chen, J. Wang, J. Chen, and W. He, "A MEMS based electrochemical vibration sensor for seismic motion monitoring," *J. Microelectromech. Syst.*, vol. 23, no. 1, pp. 92–99, Feb. 2014, doi: 10.1109/JMEMS.2013.2292833.

[3] F. Li, M. Valero, J. Clemente, Z. Tse, and W. Song, "Smart sleep monitoring system via passively sensing human vibration signals," *IEEE Sensors J.*, vol. 21, no. 13, pp. 14466–14473, Jul. 2021, doi: 10.1109/JSEN.2020.3013435.

[4] N. Hong et al., "High-speed rail suspension system health monitoring using multi-location vibration data," *IEEE Trans. Intell. Transp. Syst.*, vol. 21, no. 7, pp. 2943–2955, Jul. 2020, doi: 10.1109/TITS.2019.2921785.

[5] ISO 16063-11, "Methods for the calibration of vibration and shock transducers—Part 11: Primary vibration calibration by laser interferometry," *Int. Org. Standardization*, Geneva, Switzerland, 1999.

[6] ISO 16063-41, "Methods for the calibration of vibration and shock transducers—Part 41: Calibration of laser vibrometers," *Int. Org. Standardization*, Geneva, Switzerland, 2011.

[7] T. Pozar and J. Mozina, "Enhanced ellipse fitting in a two-detector homodyne quadrature laser interferometer," *Meas. Sci. Technol.*, vol. 22, Jun. 2011, Art. no. 085301, doi: 10.1088/0957-0233/22/8/085301.

[8] H.-J. von Martens, "Invited article: Expanded and improved traceability of vibration measurements by laser interferometry," *Rev. Sci. Instrum.*, vol. 84, Jun. 2013, Art. no. 121601, doi: 10.1063/1.4845916.

[9] C. S. Veldman, "A novel implementation of an ISO standard method for primary vibration calibration by laser interferometry," *Metrologia*, vol. 40, no. 1, pp. 1–8, Apr. 2003, doi: 10.1088/0026-1394/40/2/301.

[10] Y.-B. Lee, H. C. Kim, and S.-W. Kim, "Determination of the sensitivity phase of an accelerometer based on an analysis of the harmonic components of the interference signal," *Meas. Sci. Technol.*, vol. 19, Feb. 2008, Art. no. 045204, doi: 10.1088/0957-0233/19/4/045204.

[11] N. Garg, O. Sharma, A. Kumar, and M. I. Schiefer, "A novel approach for realization of primary vibration calibration standard by homodyne laser interferometer in frequency range of 0.1 Hz to 20 kHz," *Measurement*, vol. 45, pp. 1941–1950, Oct. 2012, doi: 10.1016/j.measurement.2012.04.011.

[12] D. A. Scott and L. P. Dickinson, "Distortion effects in primary calibration of low-frequency accelerometers," *Metrologia*, vol. 51, pp. 212–224, May 2014, doi: 10.1088/0026-1394/51/3/212.

[13] G. D'Emilia, A. Gaspari, and E. Natale, "Amplitude–phase calibration of tri-axial accelerometers in the low-frequency range by a LDV," *J. Sensors Sensor Syst.*, vol. 8, pp. 223–231, May 2019, doi: 10.5194/jsss-8-223-2019.

[14] M. Yang, C.-G. Cai, Z.-H. Liu, and Y. Wang, "Research on the method of the triaxial primary vibration calibration using the heterodyne interferometry," *Acta Metrologica Sinica*, vol. 39, no. 2, pp. 201–206, Mar. 2018, doi: 10.3969/j.issn.1000-1158. 2018.02.13.

[15] O. Furukawa and Y. Tanaka, "Interference signal processing for dynamic displacement measurement with 1 ns time resolution," *Appl. Phys. Express*, vol. 11, Dec. 2017, Art. no. 012501, doi: 10.7567/APEX.11.012501.

[16] X. Wang, J. Su, J. Yang, L. Miao, and T. Huang, "Investigation of heterodyne interferometer technique for dynamic angle measurement: Error analysis and performance evaluation," *Meas. Sci. Technol.*, vol. 32, Jul. 2021, Art. no. 105016, doi: 10.1088/1361-6501/ac0d77.

[17] R. Cheng, Z. Liu, G. Zhai, Q. Lv, M. Yang, and C. Cai, "High-acceleration vibration calibration system based on phase-locked resonance control," *Sensors*, vol. 22, Sep. 2022, Art. no. 7208, doi: 10.3390/s22197208.

[18] Q. Sun, T. Bruns, A. Taubner, L. Yang, A. Liu, and A. Zuo, "Modifications of the sine-approximation method for primary vibration calibration by heterodyne interferometry," *Metrologia*, vol. 46, pp. 646–654, Oct. 2009, doi: 10.1088/0026-1394/46/6/006.

[19] M. Yang, H. Zhu, C. Cai, Y. Wang, and Z. Liu, "Bandpass-sampling-based heterodyne interferometer signal acquisition for vibration measurements in primary vibration calibration," *Appl. Opt.*, vol. 57, no. 29, pp. 8586–8592, Oct. 2018, doi: 10.1364/AO.57.008586.

[20] Y. Wang et al., "Periodic nonlinear error and its compensation method in heterodyne laser interferometer," *J. Harbin Inst. Technol.*, vol. 52, no. 6, pp. 126–133, Jun. 2020, doi: 10.11918/202004024.

[21] G. Zhai, X. Yang, and Q. Lv, "A calibration system of resonant high-acceleration and metrological traceability," *Meas. Sci. Technol.*, vol. 32, Oct. 2021, Art. no. 125904, doi: 10.1088/1361-6501/ac28d1.

[22] P. Yang, G. Xing, and L. He, "Calibration of high-frequency hydrophone up to 40 MHz by heterodyne interferometer," *Ultrasonics*, vol. 54, pp. 402–407, Jul. 2014, doi: 10.1016/j.ultras.2013.07.013.

[23] T. Shimoda, W. Kokuyama, and H. Nozato, "Primary calibration system for digital accelerometers," *Metrologia*, vol. 58, Jun. 2021, Art. no. 045002, doi: 10.1088/1681-7575/ac0403.

[24] Z. Wang et al., "Digital accelerometer calibration method based on S/PDIF signal decoding," *J. Vib., Meas. Diagnosis*, vol. 41, no. 6, pp. 1176–1181, Dec. 2021, doi: 10.16450/j.cnki.issn.1004–6801.2021.06.020.

[25] M. Yang, H. Huang, Z. Liu, C. Cai, Y. Wang, and J. Yang, "Sine approximation-based comparison method for determining the phase-frequency characteristic of analog-to- digital converters," *IEEE Trans. Ind. Electron.*, to be published, doi: 10.1109/TIE.2023.3253953.

[26] Q. Sun, W. Wabinski, and T. Bruns, "Investigation of primary vibration calibration at high frequencies using the homodyne quadrature sine-approximation method: Problems and solutions," *Meas. Sci. Technol.*, vol. 17, no. 8, pp. 2197–2205, Jul. 2006, doi: 10.1088/0957-0233/17/8/020.

[27] T. Shimoda, W. Kokuyama, and H. Nozato, "Precise sinusoidal signal extraction from noisy waveform in vibration calibration," *Metrologia*, vol. 59, May 2022, Art. no. 035010, doi: 10.1088/1681-7575/ac6cba.

[28] N. Garg, K. Soni, A. Kumar, and T. K. Saxena, "Applications of laser interferometry in providing traceable vibration measurements in India," *MAPAN*, vol. 30, no. 2, pp. 91–104, Jun. 2015, doi: 10.1007/s12647-014-0124-y.
[29] W.-S. Cheung, "Effects of the sample clock of digital-output MEMS accelerometers on vibration amplitude and phase measurements," *Metrologia*, vol. 57, Jan. 2020, Art. no. 015008, doi: 10.1088/1681-7575/ab5505.
[30] N. Garg and B. S. Chauhan, "Measurement uncertainty in vibration calibration in frequency range of 5 Hz to 10 kHz," *MAPAN*, vol. 35, no. 3, pp. 397–405, Jul. 2020, doi: 10.1007/s12647-020-00385-2.
[31] N. Garg and M. Singh, "Measurement uncertainty in primary calibration of accelerometer complex sensitivity at low frequencies," *MAPAN*, vol. 36, pp. 821–831, Apr. 2021, doi: 10.1007/s12647-021-00454-0.
[32] M. Yang, H.-X. Zhao, Z.-H. Liu, H.-J. Li, and C.-G. Cai, "Calibration of low frequency accelerometer based on the Earth's gravitation method," *Acta Metrologica Sinica*, vol. 43, no. 8, pp. 1064–1069, Aug. 2022, doi: 10.3969/j.issn.1000-1158.2022.08.14.
[33] M. Yang, Y. Wang, C. Cai, Z. Liu, H. Zhu, and S. Zhou, "Monocular vision-based low-frequency vibration calibration method with correction of the guideway bending in a long-stroke shaker," *Opt. Express*, vol. 27, pp. 15968–15981, May 2019, doi: 10.1364/OE.27.015968.
[34] M. Yang, C. Cai, Z. Liu, and Y. Wang, "Monocular vision-based calibration method for determining frequency characteristics of low-frequency vibration sensors," *IEEE Sensors J.*, vol. 21, no. 4, pp. 4377–4384, Feb. 2021, doi: 10.1109/JSEN.2020.3035581.
[35] M. Yang, H. Zhu, C. Cai, Y. Wang, Z. Liu, and S. Zhou, "Monocular vision-based Earth's gravitation method used for low-frequency vibration calibration," *IEEE Access*, vol. 8, pp. 129087–129093, 2020, doi: 10.1109/ACCESS.2020.300929.
[36] M. Yang, Z. Liu, Y. Wang, C. Cai, and J. Yang, "Monocular vision-based multiparameter dynamic calibration method used for the low-frequency linear and angular vibration sensors," *IEEE Trans. Ind. Electron.*, vol. 70, no. 5, pp. 5365–5374, May 2023, doi: 10.1109/TIE.2022.3186310.
[37] JCGM 100, "Evaluation of measurement data-guide to the expression of uncertainty in measurement," *BIMP*, 2008. [Online]. Available: https://ncc.nesdis.noaa.gov/documents/documentation/JCGM_100_2008_E.pdf

Ming Yang (Member, IEEE) received the B.S. degree in measurement and control technology and instrumentation from the Department of Measurement and Control Technology and Instrumentation, Beijing University of Chemical Technology (BUCT), Beijing, China, in 2014, and the Ph.D. degree in control science and engineering from the Department of Control Science and Engineering, BUCT, Beijing, China, in 2020.

He is currently an Associate Professor with the Department of Automation, College of Electrical Engineering, Guizhou University, Guiyang, China. His research interests include laser and machine vision detection, and vibration metrology and monitoring.

Chenguang Cai received the Ph.D. degree in precision instrumentation and mechanics from the School of Instruments Science and Optoelectronic Engineering, Beihang University, Beijing, China, in 2007.

From 2007 to 2009, he was with Nokia Research Center (Beijing) as a Postdoctor. He is currently a Research Fellow with the National Institute of Metrology, Beijing, China. He was a Visiting Scientist with Physikalisch-Technische Bundesanstalt, Germany, in 2016. He is interested in vibration calibration and optics measurement.

Deguang Wang received the B.S. degree in automation and Ph.D. degree in control science and engineering from Xidian University, Xi'an, China, in 2014 and 2019, respectively.

He is currently an Associate Professor with the Department of Automation, College of Electrical Engineering, Guizhou University, Guiyang, China. His research interests include supervisory control, fault diagnosis, and privacy analysis of discrete event systems.

Qinmu Wu received the B.S. degree in automation and the M.S. degree in control science and engineering from the Guizhou University of Technology, Guiyang, China, in 1998 and 2001, repectively, and the Ph.D. degree in control science and engineering from the Huazhong University of Science and Technology, Wuhan, China, in 2007.

From 2001 to 2003, he was a worker with Huawei Technologies Company. He is currently a Professor and the M.S. Supervisor with the College of Electrical Engineering, Guizhou University, Guiyang, China. His current research interests include networked control, control theory and applications, and electric vehicle transmission control.

Zhihua Liu received the B.S. degree in mechanical engineering from the Department of Mechanical Engineering, Jilin University, Changchun, China, in 2010, and the Ph.D. degree in mechanical engineering from the Department of Mechanical Engineering, Tsinghua University, Beijing, China, in 2015.

He is currently a Vice Research Fellow with the National Institute of Metrology, Beijing, China. His research interest lies in vibration metrology, standards and calibration, transducer testing, and mechatronic design and control.

Ying Wang received the Ph.D. degree in precision instrumentation and mechanics from the School of Instruments Science and Optoelectronic Engineering, Beihang University, Beijing, China, in 2006.

From 2015 to 2016, she was a Visiting Scholar with Johns Hopkins University, America, and an Associate Professor with the Beijing University of Chemical Technology. She is currently a Professor with the Institute of Microelectronics, Chinese Academy of Sciences, Beijing, China. She is interested in machine vision and photoelectric detection.